Thermal excitation of d band electrons in Au: implications for laser-induced phase transformations

Zhibin Lin and Leonid V. Zhigilei*

Department of Materials Science and Engineering, University of Virginia
116 Engineer's Way, Charlottesville, VA 22904-4745

ABSTRACT

The temperature dependences of the electron heat capacity and the electron-phonon coupling factor are investigated for Au based on the electron density of states obtained from *ab initio* electronic structure calculations. Thermal excitation of d band electrons leads to a significant (up to an order of magnitude) increase in the electron-phonon coupling factor and makes a considerable contribution to the electron heat capacity in the range of electron temperatures typically realized in femtosecond laser material processing applications. Simulations performed with a combined atomistic-continuum method demonstrate that the increase in the strength of the electron-phonon coupling at high electron temperatures leads to a faster lattice heating, generation of stronger thermoelastic stresses, and a significant decrease in the time of the onset of the melting process. The timescale of the melting process predicted in the simulation accounting for the thermal excitation of d band electrons is in excellent agreement with the results of recent time-resolved electron diffraction experiments. A simulation performed with commonly used approximations of a constant electron-phonon coupling factor and a linear temperature dependence of the electron heat capacity, on the other hand, significantly overpredicts the time of the beginning of the melting process, supporting the importance of the electron density of states effects and thermal excitation of lower band electrons for realistic modeling of femtosecond pulse laser processing.

Keywords: Electron-phonon coupling, electron density of states, molecular dynamics, laser melting

1. INTRODUCTION

Irradiation of a solid target with an intense ultrashort (femtosecond) laser pulse has the ability to bring material to a state of strong electron-lattice nonequilibrium and trigger a cascade of coupled transient processes that include electron-phonon thermalization, nonequilibrium energy transport, as well as structural/phase transformations occurring under extreme and dynamic pressure-temperature conditions. The transient and highly nonequilibrium character of laser-induced processes makes the quantitative theoretical/computational description of the laser-materials interactions challenging. For metals, computational modeling of ultrashort-pulse laser interactions is commonly based on the two-temperature model (TTM) [1], which describes the time evolution of the lattice and electron temperatures, T_l and T_e, by two coupled non-linear differential equations:

$$C_e(T_e)\frac{\partial T_e}{\partial t} = \nabla\left[K_e(T_e,T_l)\nabla T_e\right] - G(T_e)(T_e - T_l) + S(\vec{r},t) \quad (1)$$

$$C_l(T_l)\frac{\partial T_l}{\partial t} = G(T_e)(T_e - T_l) \quad (2)$$

where C and K are the heat capacities and thermal conductivities of the electrons and the lattice as denoted by subscripts e and l, $G(T_e)$ is the electron-phonon coupling factor related to the rate of the energy exchange between the electrons and the lattice, and $S(\vec{r},t)$ is a source term describing the local energy deposition by the laser pulse. The model accounts for the laser excitation of the conduction band electrons, energy transfer to the atomic vibrations due to the electron–phonon coupling, and the electronic heat diffusion from the irradiated surface to the bulk of the target.

* lz2n@virginia.edu; Phone: (434) 234 3582; Fax: (434) 982 5660; http://www.faculty.virginia.edu/CompMat/

High-Power Laser Ablation VI, edited by Claude R. Phipps, Proc. of SPIE
Vol. 6261, 62610U, (2006) · 0277-786X/06/$15 · doi: 10.1117/12.674636

Despite numerous successful applications of TTM, the inherent limitation of the model is its inability to adequately describe the kinetics of phase transformations and changes in the microstructure occurring under highly nonequilibrium conditions induced in the target material by short pulse laser irradiation. In order to overcome this limitation we have recently developed a combined atomistic-continuum model that incorporates the classical molecular dynamics (MD) method into the general framework of the TTM model [2]. In the combined TTM-MD model, MD substitutes the TTM equation for the lattice temperature in the region of irradiated target affected by laser-induced structural transformations. The diffusion equation for the electron temperature is solved simultaneously with MD integration of the equations of motion of atoms and an additional coupling term is added to the conventional MD equations of motion in order to account for the energy exchange between the electrons and the lattice [2]. First applications of the combined TTM-MD model have provided insights into the microscopic mechanisms of laser melting and photomechanical damage in metal films and bulk targets [3,4,5,6]. Moreover, the important role of non-thermal channels of laser energy redistribution (energy transfer to the energy of collective atomic motions associated with the relaxation of laser-induced stresses and the energy of quasi-static anisotropic stresses), not accounted for in the conventional TTM model, has been revealed in TTM-MD modeling [7].

An important aspect in the application of the TTM or TTM-MD models for quantitative descriptions of the material response to the ultrashort pulse laser irradiation is the choice of adequate temperature dependent thermophysical properties of the target material. Due to the small heat capacity of the electrons, laser excitation can transiently bring the electron temperature to very high values, comparable to the Fermi temperature. At such high electron temperatures, the temperature dependent thermophysical properties of the system can be directly affected by the thermal excitation of the lower band electrons in noble and transition metals [8,9]. A detailed analysis of the connections between the electron density of states (DOS) in the target material and the temperature dependence of the electron-phonon coupling, electron heat capacity and thermal conductivity are needed for a realistic description of laser-material interactions.

In this paper, the effects of the electron DOS on thermophysical material properties are illustrated for femtosecond laser interactions with Au films. In the next section, the temperature dependences of the electron heat capacity and the electron-phonon coupling factor are analyzed based on the electronic structure calculations performed within the density functional theory. The results of the analysis of the thermophysical properties of Au at high electron temperatures are incorporated into TTM-MD model and applied for simulations of laser melting of thin Au films. The results of the simulations are presented and related to the experimental data obtained for a similar system in recent time-resolved electron diffraction experiments in Section 3. A brief summary of the results is given in Section 4.

2. THE EFFECT OF DOS AND THERMAL EXCITATION OF ELECTRONS ON THERMOPHYSICAL PROPERTIES

The effect of the thermal excitation of 5d band electrons in Au on the thermophysical properties of the material irradiated by an intense laser pulse is discussed in this section. In particular, the temperature dependences of the electron heat capacity $C_e(T_e)$ and the electron-phonon coupling factor $G(T_e)$ are analyzed in a broad range of the electron temperatures based on the electron DOS obtained from *ab initio* electronic structure calculations. The results of the calculations are compared with the predictions of the free electron gas model.

2.1 Electron DOS, chemical potential, and electron heat capacity

The electron heat capacity can be calculated by taking the derivative of the total electronic energy density with respect to the electron temperature [10]:

$$C_e(T_e) = \left(\frac{\partial u}{\partial T_e}\right)_V = \int_{-\infty}^{\infty} (\varepsilon - \varepsilon_F) \frac{\partial f(\varepsilon, \mu, T_e)}{\partial T_e} g(\varepsilon) d\varepsilon \qquad (3)$$

where μ is the chemical potential at T_e, ε_F is the Fermi energy, $g(\varepsilon)$ is the electron DOS at the energy level ε, and $f(\varepsilon, \mu, T_e)$ is the Fermi distribution function defined as $f(\varepsilon, \mu, T_e) = \{\exp[(\varepsilon - \mu)/k_B T_e] + 1\}^{-1}$. When the electron temperature is much smaller than the Fermi temperature (T_F = 64 200 K for Au [10]), only electrons at around the Fermi surface are excited and the electron heat capacity is known to be a linear function of the electron temperature, $C_e(T_e) = \gamma T_e$, where γ is the electron heat capacity constant defined, within the free electron gas model, by the free

electron density n_e and the Fermi energy ε_F, $\gamma = \pi^2 n_e k_B^{\ 2} / 2\varepsilon_F$. In particular, using the values of the free electron density and the Fermi energy from Ref. [10], the electron heat capacity constant for Au can be calculated to be γ = 62.7 $Jm^{-3}K^{-2}$. At high electron temperatures, however, lower band electrons could be excited to the conduction band, resulting in deviations from the linear temperature dependence of the electron heat capacity.

Both theoretical calculations [11,12,13] and X-ray photoemission spectroscopy experiments [14] have shown that the d band in Au, located relatively close to the Fermi level, has a rather complicated structure. In the analysis of the temperature dependence of the thermophysical properties of Au performed in [9], a square function centered at 4.8 eV below the Fermi energy with a width of 5.2 eV was used as an approximation of the d band. In order to understand to what degree the fine structure of the electron DOS would affect the temperature dependent thermophysical properties in Au, we perform the electronic structure calculation using the *Vienna Ab-initio Simulation Package* (VASP) [15] and obtain the electron DOS for Au at T_e=0 K, shown in Fig. 1. The calculation is done for the equilibrium lattice parameter, 4.166 Å, using the Vanderbilt ultrasoft pseudopotential (US) [16] where the exchange correlation term is treated within the generalized gradient approximation (GGA). It can be seen from Fig. 1 that, although the square function describes the presence of high density of states associated with d band electrons, accounting for the detailed structure of the d band, especially on the high energy side close to the Fermi level, can introduce significant corrections to the calculated number of thermally excited electrons.

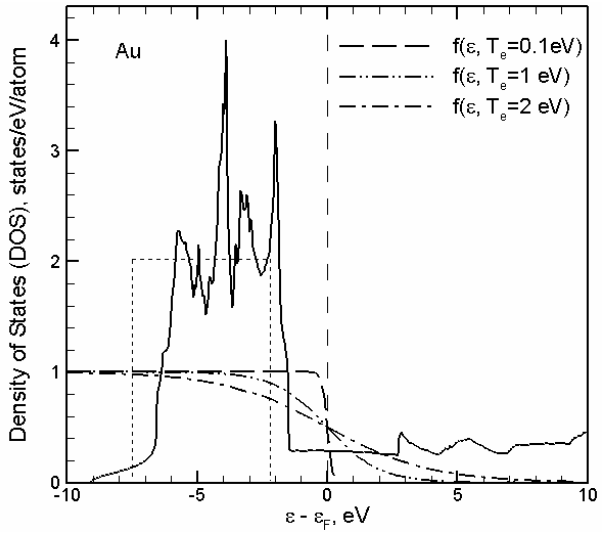

Figure 1. Electron DOS obtained in electron structure calculations performed with VASP (solid line) and a square function approximation for the 5d band in Au used in Ref. [9] (dashed line). The Fermi distribution functions are also shown for three different values of the electron temperature.

From examination of the electron DOS together with the Fermi distribution functions at various electron temperatures, it is clear that for electron temperatures less than 0.1 eV (~10^3 K) only electrons around the Fermi level are excited, while at T_e ~ 1 eV (~10^4 K) or higher, the number of excited d band electrons can be significant and should be taken into account.

In order to calculate the electron heat capacity from Eq. (3), it is necessary to evaluate the expression for $\partial f / \partial T_e$, which requires the determination of the chemical potential $\mu(T_e)$. From the conservation of the total number of electrons, one can obtain the chemical potential by setting the result of the integration of the product of DOS and the Fermi distribution function at T_e over all energy levels to be equal to the total number of electrons N_e [10],

$$N_e = \int_{-\infty}^{\infty} f(\varepsilon, \mu(T_e), T_e) g(\varepsilon) d\varepsilon \qquad (4)$$

The chemical potential obtained from Eq. (4) as a function of the electron temperature using three different approximations of DOS for Au is shown in Fig. 2. It is easy

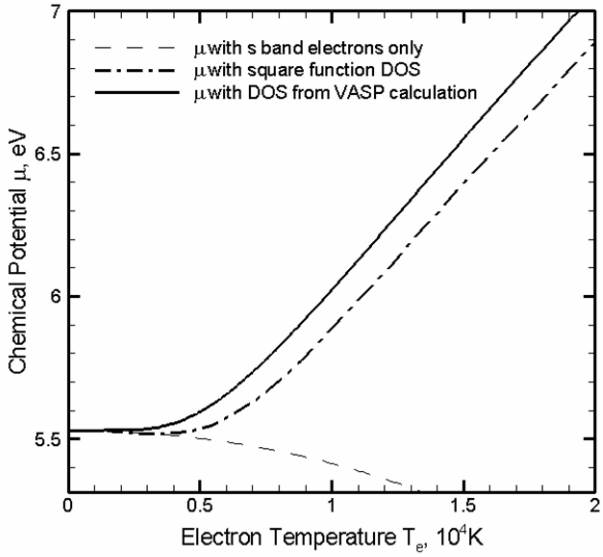

Figure 2. Chemical potential of Au as a function of the electron temperature calculated using three different approximations of DOS for Au: DOS obtained with VASP (solid line), square function approximation for the 5d band (dash-dotted line), and neglecting the contribution of the d electrons (dashed line).

to verify that with only s electrons taken into account, the chemical potential obeys the expression derived from the Sommerfeld expansion in the free electron gas model [10],

$$\mu(T_e) = \varepsilon_F \left[1 - \frac{\pi^2}{12} \left(\frac{k_B T_e}{\varepsilon_F} \right)^2 \right] \quad (5)$$

It is clear from Fig. 2 that in both calculations accounting for the presence of d band electrons, the chemical potentials agree well with the free electron gas model, Eq. (5), for T_e less than ~3000 K. However, as discussed above for Fig. 1, as T_e is increasing, the number of excited d band electrons becomes significant and the chemical potential starts to deviate from Eq. (5). In the case of the DOS calculated from VASP, the sharp increase of the number of states at energies that are higher than the high-energy edge of the square function, ε = -2.2 eV, and the contribution of d band states at around the Fermi level, Fig. 1 and Ref. [17], result in the higher values of the chemical potential as compared to the ones obtained with the square function approximation of the d band.

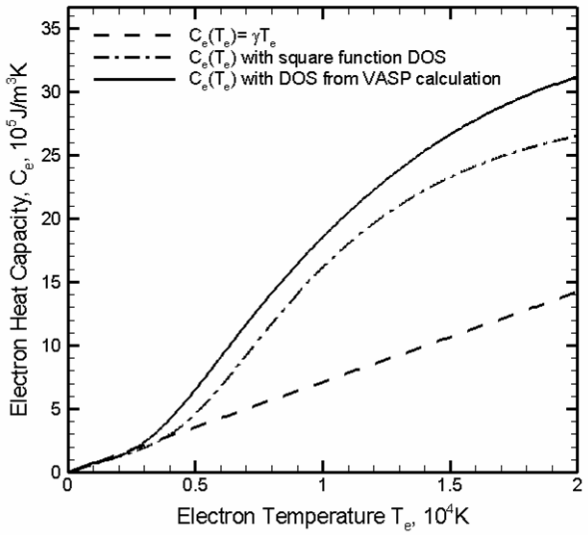

Figure 3. Electron heat capacity of Au as a function of the electron temperature calculated using $C_e = \gamma T_e$ with γ = 71 Jm^{-3}K^{-2} [18] and with the same two approximations of DOS for Au as in Fig. 2.

In Fig. 3 the temperature dependences of the electron heat capacity, calculated from Eq. (3), are shown for three approximations of DOS discussed above and used in the calculation of the chemical potential in Fig. 2. The difference in the temperature dependences of the predicted electron heat capacity can be understood from the fact that at a sufficiently high temperature significant excitation occurs from the d band in Au, which contains a large number of electron states. Calculations performed with the square function approximation of the d band give a similar temperature dependence for the electron heat capacity but underestimate the values of the heat capacity due to lack of a complete description of the d band.

Large deviations of the electron heat capacity from the linear dependence at electron temperatures that can be readily achieved by ultrashort laser pulses suggest that the application of commonly used linear approximation $C_e(T_e) = \gamma T_e$ could result in a significant overestimation of the transient values of the electron temperature during the time of the electron-lattice nonequilibrium.

The electron thermal conductivity is also affected by the thermal excitation of lower band electrons as it is related to the electron heat capacity through the Drude model relationship, $\kappa(T_e, T_l) = v_F^2 C_e(T_e) \tau_e(T_e, T_l)/3$ [10], where v_F is the Fermi velocity and $\tau_e(T_e, T_l)$ is the total electron scattering time with other electrons and the lattice. The total electron scattering time is defined by the electron-electron scattering time, τ_{e-e}, and the electron-phonon scattering time, τ_{e-ph}, and can be evaluated from the sum of the scattering rates, $1/\tau_e = 1/\tau_{e-e} + 1/\tau_{e-ph} = AT_e^2 + BT_l$, where A and B are constants [8,10]. The deviation of the electron heat capacity from the linear temperature dependence, Fig. 3, would also result in a faster electronic heat transfer during the initial stage of the electron-phonon nonequilibrium. In the example problem considered in Section 3 (laser interaction with 20 nm free standing Au film), however, a uniform distribution of the electron temperature is established in the film on the timescale of the electron-phonon thermalization and the electron thermal conductivity does not play a role in this case.

2.2 Temperature dependence of the electron-phonon coupling factor

While the electron-phonon coupling has been under active investigations in the field of superconductivity for several decades, it has also attracted a renewed interest with the fast growth of femtosecond laser applications, in which the rate of the energy transport between hot electrons and the lattice has direct implications on laser induced processes. Theoretical investigations have been focused on describing the energy exchange through electron-phonon collision

equations that characterize the phonon emission and absorption processes. The electron-phonon energy exchange within the free electron gas model was first addressed by Kaganov *et al.* [19]. It was found that the energy exchange rate could be expressed in terms of the electron relaxation time at T_e and T_l. At lattice and electron temperatures much higher than the Debye temperature and $T_e >> T_l$, the rate of the energy transfer from the electrons to the lattice per unit volume is

$$\partial E_e / \partial t = G(T_l - T_e), \quad G = \frac{\pi^2}{6}\frac{m_e C_s^{\,2} n_0}{\tau(T_e) T_e}, \tag{6}$$

where m_e is the effective electron mass, C_s is the speed of sound, n_0 is the number density of the electrons, and $\tau(T_e)$ is the electron relaxation time defined as the electron-phonon scattering time and evaluated under the assumption that the lattice temperature is equal to the electron temperature [19]. The electron-phonon scattering is proportional to the inverse of the phonon temperature and, under the condition of $T_e = T_l$, $\tau(T_e) \sim 1/T_e$, leading to a constant value of the coupling factor given by the Kaganov's expression [1].

While a constant value for the electron-phonon coupling factor is used in most of current computational and theoretical studies of short-pulse laser interactions with metals, there is growing experimental evidence suggesting that the applicability of the constant electron-phonon coupling may be limited to low laser intensities (low electronic temperatures). For example, the coupling constant is used as a fitting parameter in Ref. [20] to obtain an agreement between the calculated and experimental values of the ablation threshold in Au, whereas an empirical $G(T_e)$ dependence is introduced in Ref. [21] to provide a good description of electron photoemission data.

Several approaches have been proposed in order to account for the temperature dependence of the electron-phonon coupling factor. Based on the Kaganov's expression for the electron-phonon energy exchange rate, Eq. (6), Chen *et al.* [22] introduced a phenomenological model in which both electron-electron and electron-phonon scattering rates are included in the evaluation of the electron relaxation time, $\tau(T_e)$ in Eq. (6). The electron-electron scattering, indeed, starts to significantly contribute to the total electron scattering rate at high electron temperatures, above ~1 eV. While this contribution directly affects the electron transport properties (thermal and electrical conductivities), the relevance of the electron-electron scattering to the electron-phonon coupling factor is questionable. Similarly, the evaluation of the electron relaxation time $\tau(T_e)$ based on the temperature dependence of the electrical or thermal conductivity [1,23,24] includes the contribution of electron-electron scattering and is inappropriate for the calculation of the electron-phonon coupling at high electron temperatures.

As discussed above, in Section 2.1, in the high electron temperature regime, a quantitative analysis of the electron relaxation dynamics in metals with low-laying d bands should go beyond the free electron model and should include the consideration of the electron DOS effects. Thus, the discussion provided in Section 2.1 for the electron heat capacity and chemical potential should be extended to the electron-phonon coupling. A general description of the electron-phonon energy exchange involving arbitrary electron DOS was developed by Allen [25] based on the electron-phonon collisions equations. The rate of the energy exchange between the electrons and the lattice can be then expressed as

$$\left[\frac{\partial E_e}{\partial t}\right]_{ep} = \frac{4\pi}{\hbar N_c}\sum_{k,k'} \hbar\omega_Q \left|M_{kk'}\right|^2 S(k,k')\delta(\varepsilon_k - \varepsilon_{k'} + \hbar\omega_Q) \tag{7}$$

where $M_{kk'}$ is the electron-phonon scattering matrix element [26], N_c is the number of unit cells in the sample, k and Q denote the electron and phonon quantum numbers, respectively. $S(k,k') = (F_k - F_{k'})N_Q - F_{k'}(1 - F_k)$ is the so-called thermal factor that characterizes the phonon absorption and emission processes in the electron-phonon scattering, where F_k and N_Q are the Fermi-Dirac and Bose-Einstein distribution functions, respectively. Assuming that near room temperature only electron states around the Fermi energy contribute to the scattering processes, Eq. (7) can be rewritten in terms of the "electron-phonon spectral function" $\alpha F^2(\Omega)$ from the superconductivity theory [25]:

$$\left[\frac{\partial E_e}{\partial t}\right]_{ep} = 2\pi N_c g(\varepsilon_F)\int_0^\infty \alpha F^2(\Omega)(\hbar\Omega)^2[N(\Omega,T_l) - N(\Omega,T_e)]d\Omega \tag{8}$$

By defining $\partial E_e / \partial t = G_e(T_e)(T_l - T_e)$ and making a Taylor expansion of Eq. (8) in terms of $\hbar\Omega / k_B T_e$ and $\hbar\Omega / k_B T_l$, one could obtain the electron-phonon coupling constant: $G_0 = \pi\hbar k_B \lambda \langle \omega^2 \rangle g(\varepsilon_F)$, where λ is the electron-phonon coupling constant used in the superconductivity theory and $<\omega^2>$ is the second moment of the phonon spectrum defined by McMillan [27]. For Au, with the value $\lambda<\omega^2>=23\pm4$ meV^2 measured in Ref. [28] and DOS shown in Fig. 1, we can determine the room temperature electron-phonon coupling constant, G_0 = 2.5×10^{16} Wm^{-3}K^{-1}, which is consistent with the one obtained from reflectivity experiments: $G=(2.2\pm 0.3)\times10^{16}$ Wm^{-3}K^{-1} at low electron temperatures (a few thousand K) [18].

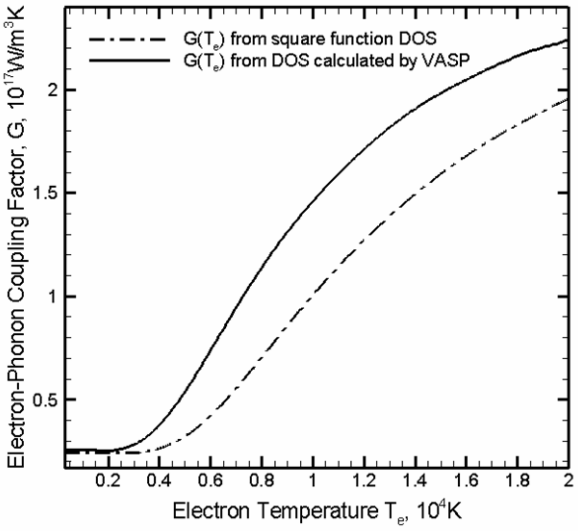

Figure 4. Electron-phonon coupling factor as a function of the electron temperature calculated for DOS obtained with VASP (solid line) and square function approximation for the 5d band (dash-dotted line).

For high T_e situations, it is necessary to take into account the electron energy dependence of the electron-phonon spectral function, i. e. $\alpha F^2(\varepsilon, \varepsilon', \Omega)$. In order to explicitly account for the d band electrons in Au, Wang *et al.* [8] proposed an approximation of the spectral function based on the assumption that the magnitude of $M_{kk'}$ is independent of the electron states, which leads to: $\alpha F^2(\varepsilon, \varepsilon', \Omega) = [g(\varepsilon)g(\varepsilon') / g^2(\varepsilon_F)]\alpha F^2(\varepsilon_F, \varepsilon_F, \Omega)$. An expression for the temperature dependent electron-phonon coupling factor could be then obtained using the approach discussed in Ref. [25]:

$$G(T_e) = \frac{\pi\hbar k_B \lambda \langle \omega^2 \rangle}{g(\varepsilon_F)} \int g^2(\varepsilon)(-\frac{\partial f}{\partial \varepsilon})d\varepsilon \qquad (9)$$

It is easy to verify that at low electron temperatures, $-\partial f / \partial \varepsilon$ reduces to a delta function and Eq. (9) gives a constant value, recovering the expression G_0 given by Allen, whereas at high electron temperatures, $-\partial f / \partial \varepsilon$ for ε away from ε_F can no longer be neglected, leading to a temperature dependence of the electron-phonon coupling factor.

The results for $G(T_e)$ in Au obtained with Eq. (9) using two different descriptions of the d band electrons discussed in Section 2.1, are shown in Fig. 4. In both cases the electron-phonon coupling factor remains approximately constant at T_e below ~3000 K. This observation is consistent with the results shown in Figs. 2 and 3 for the electron heat capacity and chemical potential, where the contribution from the thermal excitation of the d band electrons also becomes significant only when T_e becomes larger than ~3000 K. This fact also implies that at low excitation levels, where the electron temperature only reaches several thousand K, the assumption of the constant electron-phonon coupling factor provides a very good description of the rate of the electron-lattice energy exchange. However, as the electron temperature increases above ~3000 K, the value for the electron-phonon coupling factor with the full description of the electron DOS starts to significantly deviate from the constant value. The electron-phonon factor calculated with the full description of DOS exceeds the room temperature value by a factor of 5.8 at $T_e = 1\times10^4$ K and by a factor of 8.9 at $T_e = 2\times10^4$ K. As apparent from Fig. 4, the detailed description of electron DOS obtained in the electronic structure calculation gives a consistently higher value of the electron-phonon coupling than the one using the square function approximation for d band electrons.

A significant increase in the electron-phonon coupling in the range of electron temperatures typically realized in femtosecond laser material processing applications may lead to important practical implications. The faster energy transfer from the hot electrons to the lattice can result in the thermal energy confinement in a smaller surface region of the irradiated target, generation of stronger thermoelastic stresses, reduction of the threshold fluences for the onset of laser melting and ablation, and changes in the timescales of the laser induced phase transformations. Some of the implications of the temperature dependence of the thermophysical parameters discussed in this section are illustrated in the TTM-MD simulations presented in Section 3.

3. TTM-MD SIMULATIONS OF LASER MELTING OF A THIN Au FILM

In order to test the effect of the modified temperature dependence of the electron heat capacity and the electron-phonon coupling factor discussed above on the material response to the ultrashort pulse laser irradiation, we incorporated the results illustrated in Figs. 3 and 4 into the TTM-MD computational model [2] and performed simulations of laser melting of a 20 nm freestanding Au film. The conditions of the simulations are chosen to be similar to the ones realized in recent time-resolved electron diffraction experiments performed in the transmission mode for thin freestanding films [29]. The results of the simulations obtained with and without taking into account the DOS effects are related to the experimental observations.

3.1 Computational model

Simulations of laser melting of a 20 nm freestanding Au film irradiated by a 200 fs laser pulse at an absorbed fluence of 92.5 J/m^2 are performed with a combined TTM–MD model described in details elsewhere [2]. Briefly, the model is based on the TTM equations in which the classical MD method substitutes the TTM equation for the lattice temperature, Eq. (2). The equation for the electron temperature, Eq. (1), is solved by a finite difference method simultaneously with the MD integration of equations of motion of atoms. The electron temperature enters a coupling term that is added to the MD equations of motion to account for the energy exchange between the electrons and the lattice. The cells in the finite difference discretization are related to the corresponding volumes of the MD system and the local lattice temperature is defined for each cell from the average kinetic energy of the thermal motion of atoms.

Irradiation by a laser pulse is represented in the continuum part of the model by a source term with a Gaussian temporal profile. The electron mean free path in Au is larger than the optical penetration depth and the ballistic energy transport defines the effective laser energy deposition depth, estimated to be on the order of 100 nm [18]. This depth of effective electronic excitation exceeds the thickness of the Au film considered in this work, 20 nm. The reflection of the ballistic electrons from the back surface of the film results in a uniform distribution of the electronic temperature established on the timescale of the electron thermalization. The effect of the ballistic energy transport and the finite size of the film are accounted for in the source term describing the laser irradiation [2].

The initial MD computational cell is an FCC crystal, consisting of 80,000 atoms with dimensions of 8.18×8.18×20.46 nm and periodic boundary conditions imposed in the directions parallel to two (001) free surfaces. The periodic boundary conditions simulate the situation in which the laser spot diameter is sufficiently large so that the energy redistribution in the lateral directions, parallel to the free surfaces of the film, can be neglected on the time-scales considered in the simulations. An additional simulation with a larger, 20.46×20.46×20.46 nm, MD computational cell consisting of 500,000 atoms is also performed to provide a better visual picture of the melting process. The interatomic interaction in the MD part of the model is described by the embedded atom method (EAM) [30]. The choice of the interatomic potential defines all the thermal and elastic properties of the material. Thermodynamic properties of the EAM Au relevant to the laser heating and melting processes are given in Ref. [4]. Before applying laser irradiation, all systems are equilibrated at 300 K and zero pressure.

To illustrate the practical implications of effect of the electron DOS on the thermophysical parameters of the material discussed in Section 2, the TTM-MD simulations were performed for three sets of parameters of the TTM equation for the electron temperature. One simulation was performed for the parameters that correspond to the free electron gas model with only s band electrons taken into account. In this case the linear temperature dependence of the electronic heat capacity, $C_e = \gamma T_e$ with $\gamma = 71$ Jm^{-3}K^{-2} (Fig. 3), and a constant electron-phonon coupling constant taken as the room temperature value calculated from the Allen's expression (Eq. 8), $G_c = 2.5\times10^{16}$ Wm^{-3}K^{-1} are used. In two other simulations, the temperature dependences of the electron heat capacity and the electron-phonon coupling factor accounting for thermal excitations of the d band electrons and calculated with the square function approximation for the d band in one case and with the detailed DOS obtained with VASP in another case (Figs. 3 and 4) are used.

3.2 Transient evolution of electron and lattice temperatures

The evolution of the lattice and electron temperatures, predicted in TTM-MD simulations, is shown for three different treatments of the electron DOS for Au in Fig. 5. The maximum electron temperature achieved by the end of the laser pulse is significantly, by ~35%, overestimated in the model where the conventional linear dependence of the heat capacity on electron temperature is used. As discussed in Section 2.1 and illustrated in Fig. 3, the contribution of

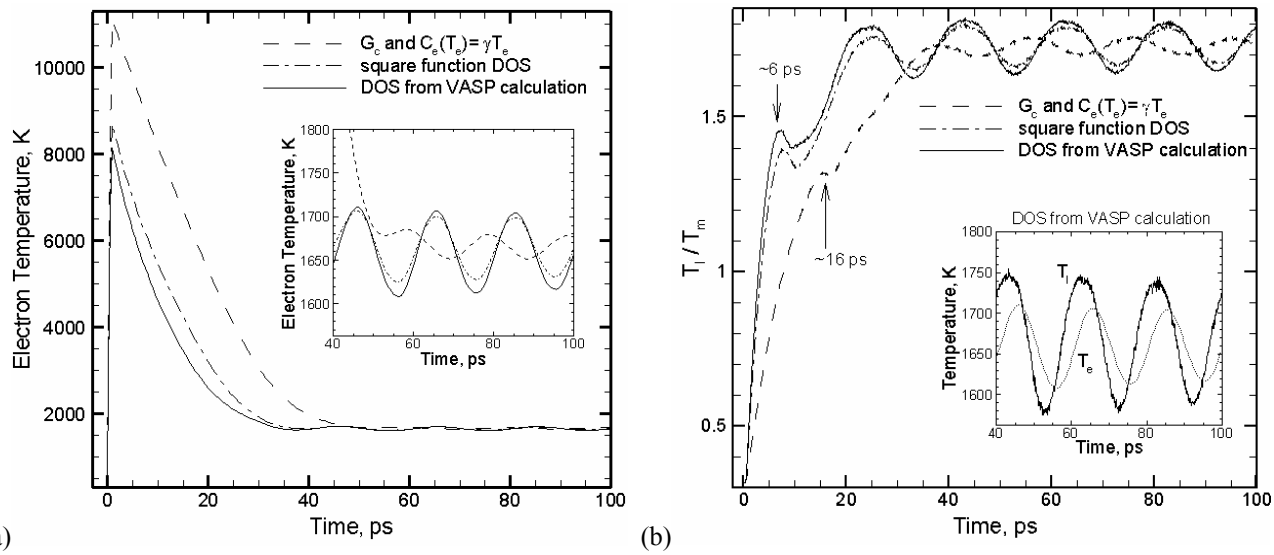

(a) (b)

Figure 5. Evolution of the electron (a) and lattice (b) temperatures in 20 nm Au film irradiated with a 200 fs laser pulse at an absorbed fluence of 92.5 J/m^2. The lattice temperature in (b) is normalized to the equilibrium melting temperature of EAM Au. The temperatures are averaged over the thickness of the film. The arrows show the time of the onset of melting. The parameters used in the simulations are calculated using three different approximations of DOS for Au: DOS obtained with VASP (solid line), square function approximation for the 5d band (dash-dotted line), and neglecting the contribution of the d electrons (dashed line), as shown in Figs. 3 and 4.

the 5d band electrons to the electron heat capacity becomes significant at high electron temperatures and results in smaller values of the electron temperature during the time of the initial electron-lattice equilibration, Fig. 5a.

The rate of the initial increase of the lattice temperature, shown in Fig. 5b, is also significantly affected by the choice of the approximation used in the model. In the simulations that account for the temperature dependence of the electron-phonon coupling (Fig. 4), the lattice temperature rise is much faster, the time when the onset of the fast homogeneous melting of the film is observed shifts from ~16 ps to ~6 ps, and the time of the saturation of the lattice temperature decreases from ~35 ps to ~20 ps.

While the evolution of the electron and lattice temperatures reflects the rate of the energy exchange between the electrons and the lattice, the electron energy profiles shown in Fig. 6 provide more direct information on the electron-phonon energy transfer rate and the time of the electron-lattice equilibration. It is apparent from Fig. 6 that the energy transfer is much faster when the thermal excitation of the d band electrons is taken into account and the temperature dependent electron-phonon coupling factor is used in the TTM-MD simulations. Based on the electron energy plots, the electron-phonon equilibration time can be estimated to be 33 ps, 35 ps, and 50 ps for the three plots shown in Fig. 6.

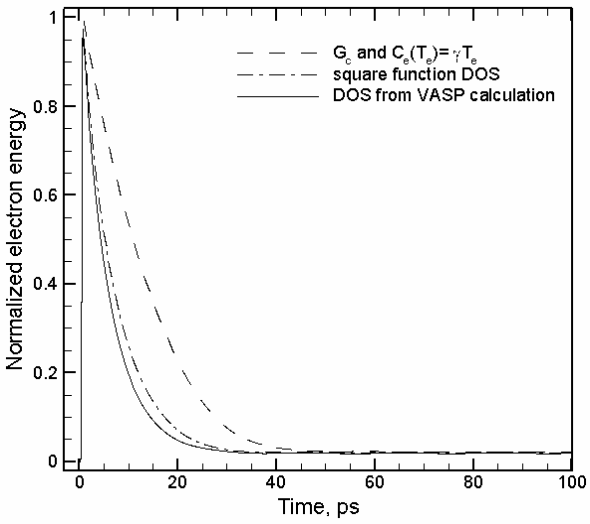

Figure 6. Evolution of the electron energy in the same three simulations illustrated in Fig. 5. The electron energies are normalized to the total laser energy absorbed by the film, $E_{tot} = F_{abs} S$, where S is the surface area of the TTM-MD computational cell, and F_{abs} is the absorbed laser fluence.

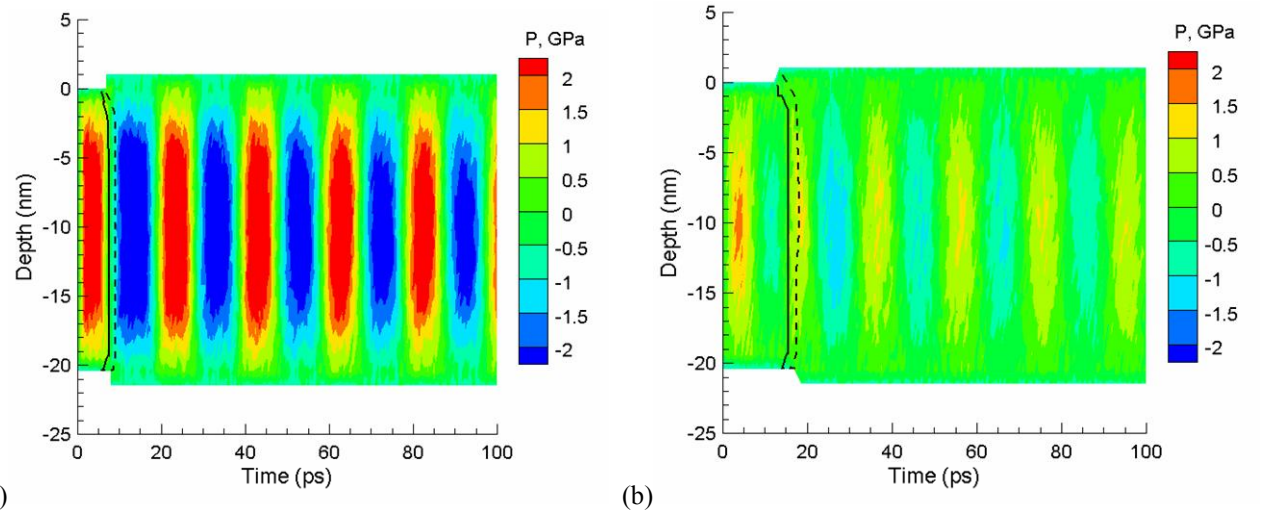

Figure 7. Contour plots showing the spatial and temporal evolution of pressure in simulations of laser melting of a 20 nm Au film irradiated with a 200 fs laser pulse at an absorbed fluence of 92.5 J/m^2. The simulations are performed with two sets of parameters: (a) $C_e(T_e)$ and $G(T_e)$ calculated with DOS from VASP and shown by solid lines in Figs. 3 and 4; (b) $C_e = \gamma T_e$ with $\gamma = 71$ Jm^{-3}K^{-2} and $G_c = 2.5\times10^{16}$ Wm^{-3}K^{-1}. Solid and dashed lines show the beginning (90% of the crystal phase, as defined by the local order parameter [2]) and the end (10% of the crystal phase) of the melting process. Laser pulse is directed along the Y-axes, from the top of the contour plots. The stepwise shape of the contour plot boundaries is related to the discretization of the mesh over which the average temperature and pressure values are calculated.

Although the initial electron-phonon equilibration of the deposited laser energy is completed by 33-50 ps after the laser pulse, the insets in Fig. 5 show long-term oscillations of the lattice and electron temperatures. The oscillations are stronger in the simulations where d band electrons are taken into account and a temperature dependent electron phonon coupling factor is used. The temperature oscillations can be related to the relaxation of the laser-induced thermoelastic stresses. The pressure contour plot in Fig. 7 shows that the fast lattice heating results in the build up of a compressive stresses inside the film within the first ~5 ps. For a 20 nm freestanding Au film, 5 ps corresponds to the time of the mechanical relaxation, i. e. the time needed for two unloading waves to cross a half of the depth of the film. During the first several picoseconds the lattice heating takes place under conditions of the inertial stress confinement [5], leading to the buildup of compressive stresses in the central part of the film, Fig. 7. The initial compressive pressure drives the expansion of the film, with tensile stresses concentrating in the central part of the film. The following gradually dissipating oscillations of the film continue beyond the time of the simulation. The oscillation of the lattice and electron temperatures shown in the insets in Fig. 5, are directly related to the pressure oscillations in Fig. 7. Compression leads to the increase of the lattice temperature whereas expansion corresponds to cooling. The electronic temperature lags behind the lattice temperature oscillations, inset in Fig. 5b, with the delay defined by the strength of the electron-phonon coupling. Quantitative thermodynamic analysis performed in Refs. [2,3] confirms that the temperature variations with pressure can be attributed to the adiabatic/isentropic expansion of the film.

As discussed above, the characteristic time of the mechanical relaxation of the film is ~5 ps and, therefore, the amount of energy transferred from the hot electrons to the lattice during this time defines the magnitude of the initial compressive pressure and the amplitude of the pressure oscillations. The fraction of the laser energy transferred from the electrons to the lattice during the first 5 ps can be obtained from the electron energy plots shown in Fig. 6 and is 54% in the simulation performed with parameters that account for the DOS effects and 23% in the simulation performed with a constant electron-phonon coupling factor and a linear temperature dependence of the electron heat capacity. As a result, in the former simulation the fast transfer of more than a half of the deposited laser energy to the thermal energy of atomic motions during the first 5 ps takes place under conditions of the inertial stress confinement and leads to the buildup of strong compressive stresses, Fig. 7a, whereas in the latter simulation the film expands during the lattice heating, the initial pressure is weak and the oscillations can be hardly observed in Fig. 7b.

The difference in the pressure oscillations in Fig. 7 is reflected in the difference in the temperature oscillations in Fig. 5, where much weaker temperature oscillations are observed in the simulation performed with parameters that do not account for the effect of the d band electrons. Note that at lower laser fluences, below the threshold for laser melting, the laser-induced elastic oscillations of the film would result in periodic oscillations of the diffraction peak positions – the effect that has been recently predicted in simulations [31] and observed in time-resolved electron diffraction experiments [32].

3.3 Ultrafast melting process

The atomic-level picture of the melting process predicted in a TTM-MD simulation using $C_e(T_e)$ and $G(T_e)$ calculated with DOS from VASP is presented in Fig. 8. The visual analysis of the snapshots taken during the melting process shows that at ~6 ps the growth of liquid regions first occurs at two free surfaces of the film, where the kinetic energy barrier is absent for liquid nucleation. However, due to the fast rate of the lattice heating, the propagation of melting fronts from the free surfaces of the film does not make any significant contribution to the overall melting process. By the time of 6 ps, the lattice temperature exceeds the overheating that corresponds to the limit of the crystal stability of the EAM Au, $\alpha=T/T_m \sim 1.25$ [2], leading to a spontaneous homogeneous nucleation of a large number of small liquid regions throughout the film and a rapid collapse of the crystalline structure within the subsequent 3-4 ps.

As discussed in Refs. [2,4], the relative contribution of the homogeneous and heterogeneous melting mechanisms in laser melting is controlled by the rate of the lattice heating and the temperature dependent velocity of the propagation of the melting fronts from the free surfaces of the film. The value of laser fluence used in the simulations presented in this paper significantly, by ~75%, exceeds the fluence needed for the complete melting of a 20 nm Au film [4]. At this level of laser excitation, the fast homogeneous melting within 3-4 ps, similar to the one illustrated in Fig. 8, is also observed in the simulation performed with a smaller constant value of the electron-phonon coupling factor. A large difference between the simulations performed with and without taking into account the effect of the thermal excitation of d band electrons, however, is found in the time of the onset of the melting process.

The difference in the time of the beginning of the melting process is apparent from Figs. 5b and 7, where the onsets of melting are marked by arrows and solid lines, respectively. A more clear representation of the timescales of the melting process is given in Fig. 9, where the evolution of the fraction of the crystal phase is shown for simulations performed with two sets of $C_e(T_e)$ and $G(T_e)$ parameters. In the case of constant G and γ, the melting starts at ~13 ps, the fraction of atoms in the liquid phase reaches 10% by 15 ps, 90% by 18 ps, and the crystalline regions completely disappear by 19 ps. In the simulation performed with $C_e(T_e)$ and $G(T_e)$ predicted using the electron DOS obtained in electronic structure calculation, the melting starts at ~6 ps, the fraction of atoms in the liquid phase reaches 10% by 7 ps, 90% by 9 ps, and the crystalline regions completely disappear by 10 ps.

The large difference in the starting time of the melting process observed between the two simulations discussed above provides a good opportunity for experimental verification of theoretical models discussed in Section 3. In particular, the results of the simulations discussed in this section can be directly related to recent time-resolved electron diffraction measurements performed for a 20 nm Au film irradiated by a 200 fs laser pulse at an absorbed laser fluence of 119 J/m^2 [29]. In order to quantitatively relate the simulation conditions to the experimental ones, we use the same overheating parameter $\alpha=T/T_m=1.9$ as in the experiment. The overheating parameter is defined as a ratio of the maximum achievable lattice temperature (obtained under the assumption that no melting occurs) to the equilibrium melting temperature, T_m [33]. Using the thermodynamic parameters of the EAM Au material [4], the value of the absorbed fluence corresponding to $\alpha=1.9$ is found to be 92.5 J/m^2 [34]. The experimental results show the presence of the long-range correlations in the diffraction profiles up to ~7 ps and the fast disappearance of the diffraction peaks corresponding to the crystal ordering during the time between 7 ps and 10 ps [29]. These experimental observations are in excellent agreement with the simulation results accounting for the thermal excitation of d band electrons. We can conclude, therefore, that the commonly used approximations of the constant electron-phonon coupling factor and the linear temperature dependence of the electron heat capacity are not appropriate for a realistic description of ultrashort pulse laser-material interactions in the high-fluence regime, where electron DOS effects start to play an important role in defining the timescales and other parameters of laser-induced processes.

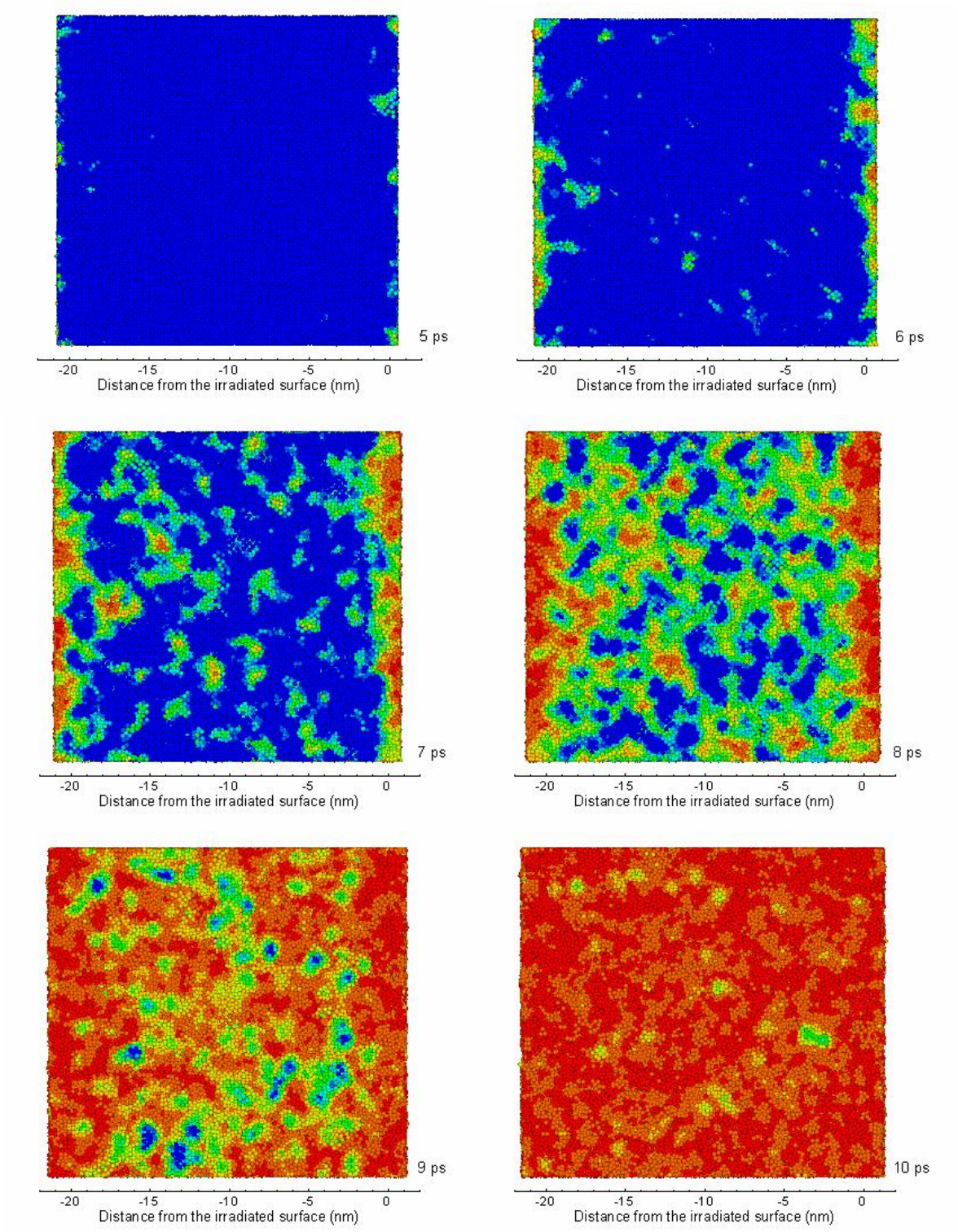

Figure 8. Snapshots of atomic configurations during the melting process in a 20 nm Au film irradiated with a 200 fs laser pulse at an absorbed fluence of 92.5 J/m^2. Atoms are colored according to the local order parameter - blue atoms have local crystalline surroundings, red atoms belong to the liquid phase. The laser pulse is directed from the right to the left sides of the snapshots. The simulation is performed with $C_e(T_e)$ and $G(T_e)$ calculated with DOS from VASP.

In this study no attempt has been made to account for the change in the electron DOS due to the modification of the electronic structure at high electron temperatures. The modifications of the electron structure would not affect the essential physics responsible for the change of the electron heat capacity and electron-phonon coupling caused by the thermal excitation of lower band electrons. Moreover, in the irradiation regime considered in this work the effect of the variations of the electron DOS on the calculated physical properties is small. Recent investigation of the modification of the electronic structure at much higher electron temperatures (~6 eV) [35] shows that the d band shifts towards lower energies while the width of the d band decreases. As a result, the contribution from the thermal excitation of d band electrons to the electron heat capacity and the electron-phonon coupling factor can be expected to be reduced at these extreme electron temperatures. In the case of transition metals, such as Ni or Pt, due to the unfilled d states in the electronic configurations, the Fermi level cuts through the d band [10]. Thus, the effect of the thermal excitation of electrons at high electron temperatures could affect the electron heat capacity and electron-phonon coupling in a very different way as compared to what is discussed in Section 3 for Au. In particular, the electron heat capacity would be smaller than the values given by the linear dependence on the electron temperature, as shown for Pt in Ref. [12], while the thermal excitation of electrons may lead to the decrease of the electron-phonon coupling with increasing electron temperature [36].

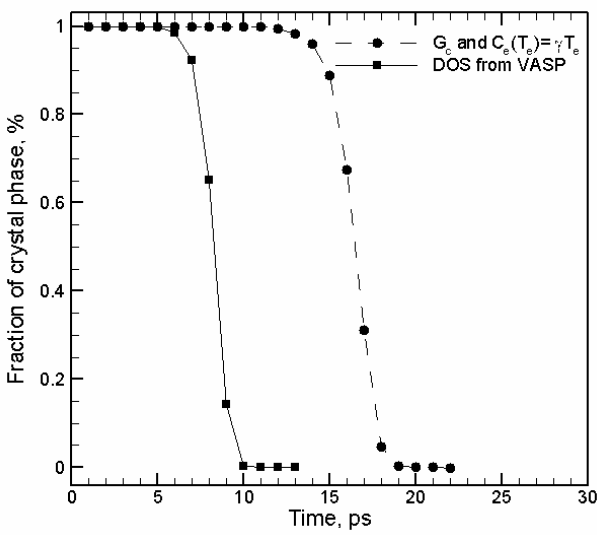

Figure 9. The evolution of the fraction of the crystal phase as a function of time in simulations performed with two sets of parameters: (Solid line) $C_e(T_e)$ and $G(T_e)$ calculated with DOS from VASP; (Dashed line) $C_e=\gamma T_e$ with $\gamma = 71$ $Jm^{-3}K^{-2}$ and $G_c = 2.5\times10^{16}$ $Wm^{-3}K^{-1}$. The atoms in the crystal phase are distinguished from the ones in the liquid phase based on the local order parameter.

4. SUMMARY

The temperature dependences of the electron-phonon coupling factor and the electron heat capacity are investigated for Au based on the electronic structure calculation performed within the density functional theory. Thermal excitation of d band electrons leads to a significant (up to an order of magnitude) increase in the electron-phonon coupling factor and makes a considerable contribution to the electron heat capacity in the range of electron temperatures typically realized in femtosecond laser material processing applications. The results of the analysis of the thermophysical properties of Au at high electron temperatures are incorporated into TTM-MD model and applied for simulations of laser melting of thin Au films. The increase in the strength of the electron-phonon coupling at high electron temperatures leads to a faster lattice heating, generation of stronger thermoelastic stresses and a higher amplitude of long-term oscillations of the film thickness, as well as significant changes in the time of the onset of the melting process. The latter can be directly related to the results of recent time-resolved electron diffraction experiments. The experimental time of the melting onset and the duration of the melting process are in excellent agreement with the results of the simulations in which the thermal excitation of d band electrons is accounted for. A simulation performed with commonly used approximations of a constant electron-phonon coupling factor and a linear temperature dependence of the electron heat capacity, on the other hand, is found to significantly (by a factor of 2) overpredict the time of the beginning of the melting process, supporting the importance of the electron DOS effects and thermal excitation of lower band electrons for realistic modeling of femtosecond pulse laser processing.

ACKNOWLEDGEMENTS

Financial support of this work is provided by the National Science Foundation through the Thermal Transport and Thermal Processes Program of the Chemical and Transport Systems Division (Award No. CTS-0348503).

REFERENCES

[1] S. I. Anisimov, B. L. Kapeliovich, and T. L. Perel'man, Electron emission from metal surfaces exposed to ultrashort laser pulses, *Sov. Phys. JETP* **39**, 375-377, 1974.

[2] D. S. Ivanov and L. V. Zhigilei, Combined atomistic-continuum modeling of short pulse laser melting and disintegration of metal films, *Phys. Rev. B* **68**, 064114, 2003.

[3] D. S. Ivanov and L. V. Zhigilei, The effect of pressure relaxation on the mechanisms of short pulse laser melting, *Phys. Rev. Lett.* **91**, 105701, 2003.

[4] Z. Lin and L. V. Zhigilei, Time-resolved diffraction profiles and atomic dynamics in short pulse laser induced structural transformations: Molecular dynamics study, *Phys. Rev. B* **73**, 184113, 2006.

[5] E. Leveugle, D. S. Ivanov, and L. V. Zhigilei, Photomechanical spallation of molecular and metal targets: molecular dynamics study, *Appl. Phys. A* **79**, 1643, 2004.

[6] L. V. Zhigilei, D. S. Ivanov, E. Leveugle, B. Sadigh, and E. M. Bringa, Computer modeling of laser melting and spallation of metal targets, *High-Power Laser Ablation V, Proc. SPIE* **5448**, 505, 2004.

[7] L. V. Zhigilei and D. S. Ivanov, Channels of energy redistribution in short-pulse laser interactions with metal targets, *Appl. Surf. Sci.* **248**, 433, 2005.

[8] X. Y. Wang, D. M. Riffe, Y. S. Lee, and M. C. Downe, Time-resolved electron-temperature measurement in a highly excited gold target using femtosecond thermionic emission, *Phys. Rev. B* **50**, 8016, 1994.

[9] A. N. Smith and P. M. Norris, Numerical solution for the diffusion of high intensity, ultrashort laser pulses within metal films, *Proceedings of 11th International Heat Transfer Conference* **5**, 241, 1998.

[10] N. W. Ashcroft and N. D. Mermin, *Solid State Physics* (Holt, Rinehart and Winston, New York, 1976).

[11] K. M. Ho and K. P. Bohnen, Stability of the missing-row reconstruction on fcc (110) transition-metal surfaces, *Phys. Rev. Lett*. **59**, 1833, 1987.

[12] T. Tsuchiya and K. Kawamura, First-principles electronic thermal pressure of metal Au and Pt, *Phys. Rev. B* **66**, 094115, 2002.

[13] F. Kirchhoff, M. J. Mehl, N. I.Papanicolaou, D. A. Papaconstantopoulos, and F.S.Khan, Dynamical properties of Au from tight-binding molecular-dynamics simulations, *Phys. Rev. B* **63**, 195101, 2001.

[14] G. K. Wertheim and D. N. E. Buchanan, Core-electron binding energies of adsorbed metallic monolayers: Au/Ag(111), *Phys. Rev. B* **33**, 914, 1986.

[15] G. Kresse and J. Hafner, Ab initio molecular dynamics for liquid metals, *Phys. Rev. B* **47**, 558, 1993.

[16] D. Vanderbilt, Soft self-consistent pseudopotentials in a generalized eigenvalue formalism, *Phys. Rev. B* **41**,7892, 1990.

[17] F. Ladstädter, U. Hohenester, P. Puschnig, and C. Ambrosch-Draxl, First-principles calculation of hot-electron scattering in metals, *Phys. Rev. B* **70**, 235125, 2004.

[18] J. Hohlfeld, S.-S. Wellershoff, J. Gudde, U. Conrad, V. Jahnke, and E. Matthias, Electron and lattice dynamics following optical excitation of metals, *Chem. Phys.* **251**, 237-258, 2000.

[19] M. I. Kaganov, I. M. Lifshitz, and L. V. Tanatarov, Relaxation between electrons and crystalline lattices, *Sov. Phys. JETP* **4**, 173, 1957.

[20] J. K. Chen and J. E. Beraun, Modeling of ultrashort laser ablation of gold films in vacuum, *J. Opt. A: Pure Appl. Opt.* **5**, 168, 2003.

[21] J. P. Girardeau-Montaut and C. Girardeau-Montaut, Theory of ultrashort nonlinear multiphoton photoelectric emission from metals, *Phys. Rev. B* **51**, 13560, 1995.

[22] J. K. Chen, W. P. Latham and J. E. Beraun, The role of electron-phonon coupling in ultrafast laser heating, *J. Laser Applications*, **17**, 63, 2005.

[23] D. Y. Tzou, *Macro- to Microscale Heat Transfer: The Lagging Behavior* (Washington, DC: Taylor & Francis, 1997).

[24] Z. G. Wang, Ch. Dufour, E. Paumier, and M. Toulemonde, The S_e sensitivity of metals under swift-heavy-ion irradiation: a transient thermal process, *J. Phys.: Condens. Matter* **6**, 6733, 1994.

[25] P. B. Allen, Theory of thermal relaxation of electrons in metals, *Phys. Rev. Lett.* **59**, 1460, 1987.

[26] J. M. Ziman, *Electrons and Phonons* (Oxford Univ. Press London, 1960).

[27] W. L. McMillan, Transition temperature of strong-coupled superconductors, *Phys.Rev.***167**, 331, 1968.

[28] S. D. Brorson, A. Kaeroonian, J. S. Moodera, D. W. Face, T. K. Cheng, E. P. Ippen, M. S. Dresselhaus and G. Dresselhaus, Femtosecond room-temperature measurement of the electron-phonon coupling constant λ in metallic superconductors, *Phys. Rev. Lett.* **64**, 2172, 1990.

[29] J. R. Dwyer, C. T. Hebeisen, R. Ernstorfer, M. Harb, V. Deyirmenjian, R. E. Jordan and R. J. D. Miller, Femtosecond electron diffraction: 'making the molecular movie', *Phil. Trans. R. Soc. A* **364**, 741, 2006.

[30] X. W. Zhou, H. N. G. Wadley, R. A. Johnson, D. J. Larson, N. Tabat, A. Cerezo, A. K. Petford-Long, G. D. W. Smith, P. H. Clifton, R. L. Martens, and T. F. Kelly, Atomic scale structure of sputtered metal multilayers, *Acta Mater*. **49**, 4005, 2001.

[31] Z. Lin and L. V. Zhigilei, Time-resolved diffraction profiles and structural dynamics of Ni film under short laser pulse irradiation, *J. Phys.: Conference Series*, in press.

[32] H. Park, X. Wang, S. Nie, R. Clinite, and J. Cao, Mechanism of coherent acoustic phonon generation under nonequilibrium conditions, *Phys. Rev. B* **72**, 100301(R), 2005.

[33] B. Rethfeld, K. Sokolowski-Tinten, D. von der Linde, and S. I. Anisimov, Ultrafast thermal melting of laser-excited solids by homogeneous nucleation, *Phys. Rev. B* **65**, 092103, 2002.

[34] In simulations, the calculation of the overheating parameter α=1.9 is done with a temperature dependent lattice heat capacity determined for the EAM Au material [4], whereas in Ref. [29] a constant heat capacity is assumed. Using an experimental temperature dependent heat capacity for Au [28], a smaller overheating factor of 1.7 can be obtained for the absorbed laser fluence of 119 J/m^2 used in the experiment [29]. Nevertheless, this discrepancy does not affect the physical interpretations and conclusions derived from the comparison of the simulations and experiments presented in this paper. In the simulation performed at a lower overheating of 1.7 with $C_e(T_e)$ and $G(T_e)$ calculated with DOS from VASP, the timescale of the melting process is very similar to the one at α=1.9: the melting starts at ~8 ps, the fraction of atoms in the liquid phase reaches 10% by 10 ps, 90% by 14 ps, and the crystalline regions completely disappear by ~15 ps.

[35] V. Recoules, J. Clérouin, G. Zérah, P. M. Anglade, and S. Mazevet, Effect of intense laser irradiation on the lattice stability of semiconductors and metals, *Phys. Rev. Lett.* **96**, 055503, 2006.

[36] Z. Lin and L. V. Zhigilei, unpublished.